J. Fluid Mech. (1968), *vol.* 31, *part* 3, *pp.* 529–546
Printed in Great Britain

Experimental and theoretical study of the stability of plane shock waves reflected normally from perturbed flat walls

By M. G. BRISCOE† AND A. A. KOVITZ

The Gas Dynamics Laboratory,
Department of Mechanical Engineering and Astronautical Sciences,
Northwestern University, Evanston, Illinois

(Received 29 June 1967)

The rate of damping of perturbations on a shock wave reflected from a perturbed flat wall was measured in a shock tube. Incident shock wave Mach numbers of 1·45 and 1·09 in air together with sinusoidal and Gaussian wall perturbations were employed. These measurements were compared with a modified form of a linearized theory due to Zaidel (1960). The linearization was performed about the basic solution of a plane shock wave reflected normally from a flat wall.

The rate of decay and the frequency and phase of oscillations agreed very well with the theoretical predictions; the amplitudes of the oscillations were somewhat larger than predicted. The reflected shock shape was initially in good agreement with theory, but higher frequency perturbations on the reflected shock front caused deviations from the predicted shape after the shock front had travelled about one wall-wavelength away from the wall.

The generally satisfactory agreement between theory and experiment supports the use of linearized analysis in predicting shock wave stability.

1. Introduction

Previous experimental studies of the stability of plane shock waves have not shown good agreement with linearized theories; this seems to be partially due to the experiments and partially due to the theories. Lapworth (1957) experimentally considered the motion of a plane shock wave through a channel containing small 'roof-top' disturbances on the walls; the consequent perturbations to the ends of the shock wave produced a different shock shape that underwent a damped oscillation and ultimately approached a planar form again. Lapworth compared his experimental results with the theory of Freeman (1957) for the same problem. Unfortunately, Freeman's solution was an asymptotic result valid many channel-diameters away from the location of the roof-tops; this, in combination with the experimental difficulties of compromising between small perturbations and perturbations that are large enough to measure, apparently prevented agreement between theory and experiment except for the frequency of the oscillations of the diffracted shock front. Both amplitude and phase of the

† Now at the von Kármán Institute for Fluid Dynamics, Rhode-Saint-Genese, Belgium.

oscillations were in poor agreement with the predictions; agreement was worse for the lower Mach numbers.

Sakharnov *et al.* (1965) studied shock waves in metal. An explosion was produced next to a block of metal; the side of the block adjacent to the explosion had a sinusoidal profile. The resulting sinusoidal shock wave propagated through the metal and was recorded photographically by a fluorometric device. They supposed that this situation could be modelled as a piston-produced shock wave according to another analysis by Freeman (1955). Rather large deviations between experimental and theoretical perturbation-damping rates were stated to be caused by the viscosity and plasticity of the metal.

The reflexion of a plane shock wave from a corrugated surface has been theoretically considered by Blackburn (1953) using a conical flow technique originated by Lighthill (1949, 1950). Blackburn's solution has two major faults with respect to performing an experiment to check its validity: the initial shock shape is assumed to be coincident with the wall shape, a statement that is clearly in conflict with an actual reflexion process, and the useful solution is only available for the far-field reflexion; i.e. many wall-wavelengths away from the wall. The experimental difficulties in measuring far-field perturbation-damping are overwhelming; a near-field solution to the shock reflexion and stability problem is very desirable.

Freeman (1955) has given an excellent discussion of shock production by the impulsive motion of a corrugated piston. He superposes conical-field solutions and obtains a complete solution to the linearized problem. Asymptotic behaviour for large time, large Mach number, and small Mach number are explicitly derived.

Zaidel (1960) also considers Freeman's piston problem. His analysis avoids conical-field solutions; rather, it reduces to the solution of a hyperbolic system of equations with boundary conditions on the moving boundaries. He also obtains a complete solution, and discusses its asymptotic behaviour with respect to large time, large Mach number, and small Mach number. For our purposes Zaidel's complete solution is preferable because it is much easier to use in conjunction with a high-speed computer. A comparison of Zaidel's complete solution with that of Freeman is not feasible; however, Zaidel shows that the low Mach number limiting cases for both are identical. We also found that Zaidel's formulation was easily extended to arbitrary wall shapes.

In the manner of Zaidel, §2 describes the theory for perturbation-damping on a shock wave reflected normally from a slightly wavy wall; §3 extends that theory to the case of an arbitrary wall shape, in particular, to reflexion from a Gaussian curve. The apparatus and experimental procedure for validating the theories are described in §4, and results and conclusions are presented in §5.

2. Linearized theory of shock reflexion from a wavy wall

When a step-shock impinges normally on a rigid *flat* wall the gas adjacent to the wall is brought to rest by an instantaneously reflected step-shock of the appropriate strength; see, for example, Courant & Friedrichs (1948, p. 152).

If, however, the step-shock impinges normally on a rigid *wavy* wall the reflexion process does not occur instantaneously (see figure 1): figure 1*b* shows the shock to be partly incident and partly reflected; figure 1*c* corresponds to the first instant when the shock front is totally reflected. The reflected front is clearly not flat. Figures 1*d* and 1*e* show schematically the expected behaviour of the reflected front with increasing time: the perturbations damp out as the reflected

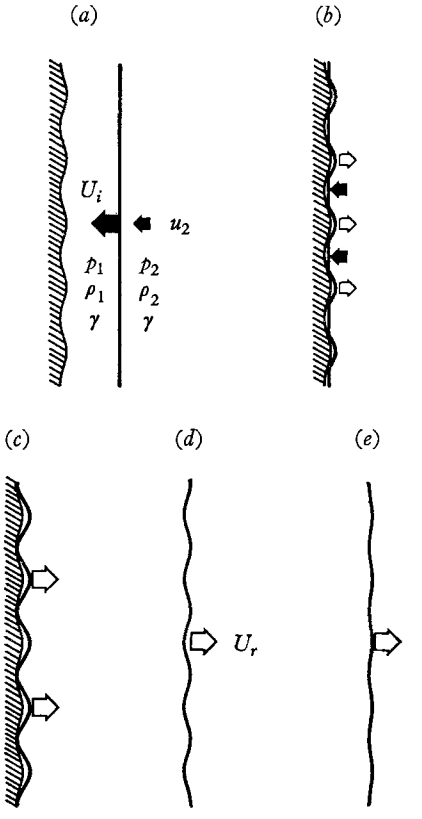

FIGURE 1. Schematic representation of shock reflexion from a wavy wall: (*a*) incident shock prior to reflexion; (*b*) early period of reflexion, containing both incident and reflected shock fronts; (*c*) instant when shock front is completely reflected; (*d*) perturbed reflected shock front, out-of-phase with wall shape; (*e*) almost flat reflected shock with perturbation in-phase with the wall.

front moves away from the wall; finally the reflected front becomes flat with a strength equal to that of a step-shock reflected from a flat wall.

The general problem, for arbitrary wall slopes, will not be attempted; rather, the wall slopes will be assumed small enough to allow all governing equations and auxiliary conditions to be linearized about the known solution for reflexion from a flat wall.

The flow in the region between the reflected shock front and the wall will be governed by the linearized Euler equations; at the shock front the Rankine–

Hugoniot equation will relate the perturbed velocities, density and pressure to the local perturbed shock velocity and shock slope.

The complete specification of the problem requires a knowledge of the flow field at some initial instant of time. We choose that initial instant to correspond to figure 1 *c*, at which time the reflected front is completely formed. For sufficiently small wall slopes, the reflected front lies everywhere very close to the wall; the perturbations in the region between the wall and the reflected front can be shown to be second order in wall slope at that instant, and are, therefore, neglected. The initial shock-front has the same wavelength as the wall, but with a different amplitude; i.e. if the wall is sinusoidal we assume that the reflected front is also sinusoidal, with a different amplitude. The above assumptions regarding the initial state are not exact; their validity will be supported by the experimental results.

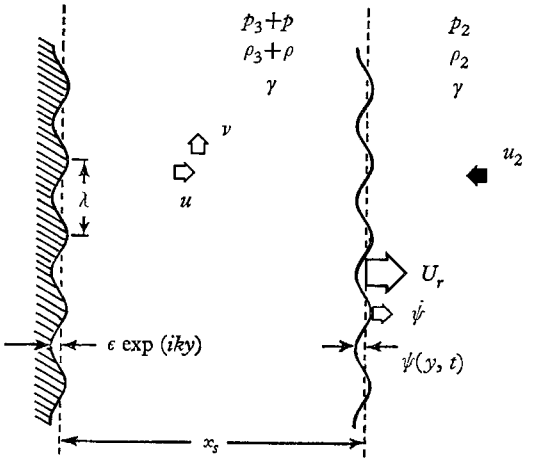

FIGURE 2. Nomenclature diagram for the linearized reflexion analysis.

An essentially equivalent linearized problem has been solved by Zaidel (1960). He considered the shock wave formed by the impulsive motion of a piston having a sinusoidal profile of small slope. In this case the initial shock shape is *exactly* the piston shape, and the initial value problem is precisely prescribed. The perturbed step-shock propagates into stationary gas; the gas between the shock front and the piston face moves according to the linearized Euler equations.

If a velocity equal and opposite to the piston velocity is imposed on the piston-shock wave-gas configuration of Zaidel's problem, we obtain a flow which is kinematically similar to that of a reflected shock-front moving away from a stationary wall. Zaidel's analysis becomes applicable in all respects, except for the assumptions necessary to establish the initial shock shape in the reflexion problem.

We shall outline the analysis for the reflexion problem, making use of Zaidel's analysis. A detailed exposition may be found in Briscoe (1967).

Figure 2 is a schematic diagram of the reflexion problem; p, ρ, $c = (\gamma p/\rho)^{\frac{1}{2}}$, u and v are pressure, density, sonic velocity and the two fluid velocities,

respectively; γ is the ratio of specific heats for a perfect gas; subscripts 1, 2 and 3 refer to the unshocked gas, the once-shocked gas, and the unperturbed twice-shocked gas (reflected region), respectively; p, ρ, u and v without subscripts are the respective perturbation quantities in the reflected region (3). U_i and $M_i = U_i/c_1$ are the incident shock speed and incident Mach number, respectively; U_r and $M_r = (U_r + u_2)/c_2$ are the unperturbed reflected shock speed and Mach number, respectively. The wall shape is given by $x_w(y) = \epsilon \exp(iky)$, with ϵ the wall amplitude and $k = 2\pi/\lambda$; λ is the wall wavelength. The real part of the complex exponential in the resulting solution will, of course, be utilized. At time t the unperturbed reflected-shock is at $x_s(t) = U_r t$; the shape of the perturbed shock is given by $\psi(y,t)$, as measured from $x_s(t)$.

The linearized Euler equations applied to region 3, for a perfect gas, take the form

$$\left.\begin{aligned} \partial u/\partial t + (1/\rho_3)(\partial p/\partial x) &= 0, \\ \partial v/\partial t + (1/\rho_3)(\partial p/\partial y) &= 0, \\ \partial p/\partial t + \gamma p_3(\partial u/\partial x + \partial v/\partial y) &= 0, \\ \partial s/\partial t &= 0, \end{aligned}\right\} \tag{2.1}$$

where s is the perturbation entropy per unit mass, and the continuity equation has been written in terms of the pressure using $c_3^2 = \gamma p_3/\rho_3$. It should be noted that the first three equations of (2.1) may be combined to form

$$\partial^2 p/\partial t^2 - c_3^2(\partial^2 p/\partial x^2 + \partial^2 p/\partial y^2) = 0;$$

if, as we shall assume, $p(x,y,t) = \bar{p}(x,t)\exp(iky)$, then we obtain

$$\partial^2 \bar{p}/\partial t^2 - c_3^2 \partial^2 \bar{p}/\partial x^2 + k^2 c_3^2 \bar{p} = 0,$$

a form of the Klein–Gordon equation (Morse & Feshbach 1953, p. 138).

The Rankine–Hugoniot jump conditions at the reflected shock-front are expressed in terms of the normal velocity relative to the front. This introduces $\dot{\psi}$ and $\partial\psi/\partial y$, where $(\cdot) \equiv \partial/\partial t + U_r(\partial/\partial x)$; $\dot{\psi}$ is the change in ψ while holding y constant, as measured relative to $x_s = U_r t$. In this case $\dot{\psi} = \partial\psi/\partial t$ since ψ is assumed not be to a function of x. After substitution of the flow properties in terms of unperturbed plus perturbed quantities the relations among the perturbation quantities, evaluated at the shock front $x = U_r t$, become

$$\left.\begin{aligned} u(U_r t, y, t) &= A\dot{\psi}, \\ p(U_r t, y, t) &= B\dot{\psi}, \\ \rho(U_r t, y, t) &= E\dot{\psi}, \\ v(U_r t, y, t) &= -u_2(\partial\psi/\partial y), \end{aligned}\right\} \tag{2.2}$$

where

$$\left.\begin{aligned} A &= 2(1 + M_r^{-2})/(\gamma+1), \\ B &= 4\rho_2(u_2 + U_r)/(\gamma+1), \\ E &= [4\rho_3/(\gamma+1)]^2/B. \end{aligned}\right\} \tag{2.3}$$

The initial shock shape at $x = t = 0$ is taken to be

$$\psi(y,0) = \epsilon(1 + U_r/U_i)\exp(iky); \tag{2.4}$$

the factor $\epsilon(U_r/U_i)$ is the distance moved by the portion of the reflected shock coming normally off the wall at $y = 0, \pm 2\lambda, \pm 4\lambda, \ldots$ during the time $2\epsilon/U_i$.

We require the fluid velocity to be tangent to the wall for all time; to first order in wall slope this demands $u(0, y, t) = 0$; from the first of (2.1) we obtain

$$u(0, y, t) = \partial p(0, y, t)/\partial x = 0. \tag{2.5}$$

The shock boundary conditions evaluated at $x = t = 0$ yield, in view of (2.5),

$$\left.\begin{aligned} v(0, y, 0) &= -u_2[\partial\psi(y, 0)/\partial y], \\ u(0, y, 0) &= p(0, y, 0) = \psi(y, 0) = 0. \end{aligned}\right\} \tag{2.6}$$

Note that the presence of the wall requires $\psi(y, 0) = 0$, which leads to $p(0, y, 0) = 0$.

The linearized problem is now completely specified in terms of (2.1), (2.2), (2.4), (2.5) and (2.6). This formulation is more explicit after elimination of the shock perturbation $\psi(y, t)$. The second and fourth of equations (2.2) may be combined, after differentiation by $\partial/\partial y$ and by $\partial/\partial t + U_r(\partial/\partial x)$, respectively, to yield a new shock boundary condition,

$$\partial v(U_r t, y, t)/\partial x = U_r^{-1}(\rho_3^{-1} - u_2/B)\,\partial p(U_r t, y, t)/\partial y, \tag{2.7}$$

where the second of (2.1) has been used to eliminate $\partial v(U_r t, y, t)/\partial t$. From the first and second of (2.2),

$$u(U_r t, y, t) = (A/B)\,p(U_r t, y, t). \tag{2.8}$$

The y-dependence is extracted from all dependent variables by the physical assumption

$$F(x, y, t) = \overline{F}(x, t)\exp(iky).$$

In accordance with Zaidel (1960), new non-dimensional independent variables, r, θ, are introduced by

$$r\cosh\theta = kc_3 t, \quad r\sinh\theta = kx;$$

or, upon solving for r and θ,

$$r = kc_3 t[1 - (x/c_3 t)^2]^{\frac{1}{2}}, \quad \theta = \operatorname{arc\,tanh}(x/c_3 t). \tag{2.9}$$

In terms of r, θ, the wall is at $\theta = 0$, and the reflected shock-front is at $\theta_0 = \operatorname{arc\,tanh}(U_r/c_3)$; the initial instant is given by $r = 0$, because $\lim_{x, t \to 0} |x/c_3 t|$ is finite for this hyperbolic problem. The dependent variables are re-named as

$$\hat{p}(r, \theta) = \overline{p}/\rho_3 c_3, \quad \hat{u}(r, \theta) = \overline{u}, \quad \hat{v}(r, \theta) = i\overline{v}.$$

Then the governing equations and auxiliary conditions may be written as

$$\left.\begin{aligned} \partial\hat{u}/\partial r + r^{-1}(\partial\hat{p}/\partial\theta) + \hat{v}\sinh\theta &= 0, \\ \partial\hat{p}/\partial r + r^{-1}(\partial\hat{u}/\partial\theta) + \hat{v}\cosh\theta &= 0, \\ \partial^2\hat{p}/\partial r^2 + r^{-1}(\partial\hat{p}/\partial r) + \hat{p} - r^{-2}(\partial^2\hat{p}/\partial\theta^2) &= 0, \end{aligned}\right\} \tag{2.10}$$

$$\hat{u}(r, 0) = \partial\hat{p}(r, 0)/\partial\theta = 0, \tag{2.11}$$

$$\left.\begin{aligned} \hat{u}(r,\theta_0) &= K_1\hat{p}(r,\theta_0), \\ \partial\hat{v}(r,\theta_0)/\partial r &= (K_2\sinh\theta_0+\cosh\theta_0)\,\hat{p}(r,\theta_0), \end{aligned}\right\} \tag{2.12}$$

$$\left.\begin{aligned} \hat{u}(0,\theta) &= \hat{p}(0,\theta) = 0, \\ \hat{v}(0,\theta) &= \hat{v}_0. \end{aligned}\right\} \tag{2.13}$$

In the above equations

$$K_1 \equiv (A/B)\rho_3 c_3, \quad K_2 \equiv (u_2\rho_3/B-1)/\beta,$$
$$\beta \equiv U_r/c_3, \quad \hat{v}_0 \equiv u_2 k\epsilon(1+U_r/U_i),$$
$$\theta_0 = \operatorname{arc\,tanh}\beta, \quad K_3 \equiv 2\sinh\theta_0(K_2\sinh\theta_0+\cosh\theta_0)-K_1.$$

Note that the last of equations (2.10) derives from the Klein–Gordon equation, introduced after (2.1).

Following Zaidel, the system of equations and auxiliary conditions in r, θ is transformed to a system in s, θ through the application of a Laplace transform,

$$G(s,\theta) \equiv \int_0^\infty g(r,\theta)\,e^{-sr}\,dr.$$

In particular, the last of equations (2.10) becomes

$$(s^2+1)(\partial^2P/\partial s^2)+3s(\partial P/\partial s)+P-\partial^2P/\partial\theta^2 = 0, \tag{2.14}$$

which does not afford any apparent simplification over its r, θ version. However, at this point Zaidel replaces the independent variable s by q through the relation $s = \sinh q$ and sets $W(q,\theta) = P\cosh q$; then (2.14) becomes the wave equation

$$\partial^2W/\partial q^2-\partial^2W/\partial\theta^2 = 0, \tag{2.15}$$

the general solution of which is $W(q,\theta) = F_1(q+\theta)+F_2(q-\theta)$. The wall boundary condition $\partial W(q,0)/\partial\theta = 0$ requires $F_1 = F_2 = F$.

The Laplace transform of the first of equations (2.10) may be written as a perfect differential, after insertion of q and W, and then integrated with respect to q:

$$-U\sinh q+[F(q+\theta)-F(q-\theta)]-V\sinh\theta = 0; \tag{2.16}$$

this equation, relating U, V and F, satisfies $U(q,0) = 0$.

On the reflected shock

$$\left.\begin{aligned} U(q,\theta_0)\cosh q &= K_1W(q,\theta_0), \\ V(q,\theta_0)\sinh q\cosh q-\hat{v}_0\cosh q &= (K_2\sinh\theta_0+\cosh\theta_0)\,W(q,\theta_0). \end{aligned}\right\} \tag{2.17}$$

Equations (2.17) relate U, V, W on the reflected shock; together with (2.16), evaluated on $\theta = \theta_0$, we obtain a difference equation relating $F(q+\theta_0)$ and $F(q-\theta_0)$. Briscoe (1967) gives the details of the solution, as obtained by Zaidel. The essential step in solving the difference equation is the assumption of a solution in the form of an infinite series of terms $B_n(\theta_0)\exp[-(2n+1)q]$; the $B_n(\theta_0)$ are determined by the difference equation after setting the coefficients of $\exp[-(2n+1)q]$ equal to zero for all n. The expression for

$$W(q,\theta) = F(q+\theta)+F(q-\theta)$$

is then

$$W(q,\theta) = \sum_{n=0}^{\infty} B_n\frac{\cosh(2n+1)\theta}{\cosh(2n+1)\theta_0}\exp[-(2n+1)q], \tag{2.18}$$

with the B_n as known constants which depend upon the unperturbed reflexion problem. They are exhibited after (2.21).

The Laplace inversion of (2.18) is straightforward since

$$\exp(-mq) = [(s^2+1)^{\frac{1}{2}} - s]^m;$$

a standard Laplace inversion yields

$$\hat{p}(r,\theta) = \sum_{n=0}^{\infty} B_n \frac{\cosh(2n+1)\theta}{\cosh(2n+1)\theta_0} J_{2n+1}(r), \tag{2.19}$$

where the $J_{2n+1}(r)$ are Bessel functions. Returning to physical variables we may obtain, on the reflected shock,

$$\overline{p}(x_s,t)/\rho_3 c_3 = \sum_{n=0}^{\infty} B_n J_{2n+1}(r_s), \tag{2.20}$$

with $r_s \equiv (kx_s/\beta)(1-\beta^2)^{\frac{1}{2}}$.

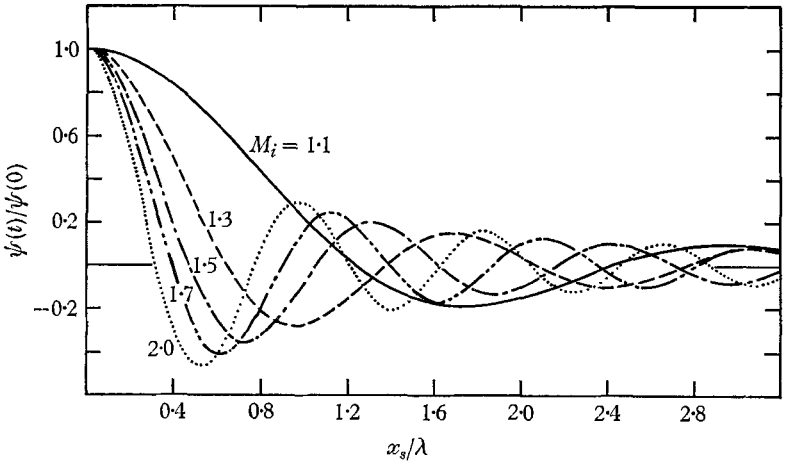

FIGURE 3. Theoretical perturbation damping for shock reflexion from a sinusoidal wall.

From the shock boundary-conditions in terms of $\psi(y,t) = \overline{\psi}(t)\exp(iky)$ we may now perform a time-integration and develop the reflected shock shape as

$$\overline{\psi}(r_s)/\overline{\psi}(0) = \sum_{n=0}^{\infty} B_n \int_{r_s}^{\infty} J_{2n+1}(x)\,dx \Big/ \sum_{n=0}^{\infty} B_n.$$

A form which is particularly suitable for computation was stated by Zaidel, and described in more detail by Nikolaev (1965) and Briscoe (1967); it is

$$\overline{\psi}(r_s)/\overline{\psi}(0) = J_0(r_s) + \sum_{n=1}^{\infty} D_n J_{2n}(r_s) \Big/ \sum_{n=0}^{\infty} B_n, \tag{2.21}$$

with

$$D_n = (K_1+K_3)^{-1}\{[K_1+\tanh(2n+1)\theta_0]B_n - B_{n-1}[K_1-\tanh(2n-1)\theta_0]\},$$

$$B_0 = -2\hat{v}_0 \sinh\theta_0/(K_1+\tanh\theta_0),$$

$$B_1 = B_0[(K_1-2K_3)+\tanh\theta_0]/(K_1+\tanh 3\theta_0)$$

and

$$B_{n+1}[K_1+\tanh(2n+3)\theta_0] + 2B_n K_3 + B_{n-1}[K_1-\tanh(2n-1)\theta_0] = 0.$$

Zaidel's results appear with a minus sign in front of the series in (2.21). Computation shows that the series term is not negligible; therefore, the apparently typographical sign difference is significant. Our experimental results will be seen to agree well with (2.21).

Equation (2.21) is plotted in figure 3 for several incident Mach numbers. We see that the damping behaviour is dominated by $J_0(r_s)$. As $M_i \to 1$ the first zero-crossing of $\overline{\psi}/\overline{\psi}(0)$ is found at very large values of x_s/λ. In §4 the experimental results will be seen to compare favourably with these analytical curves.

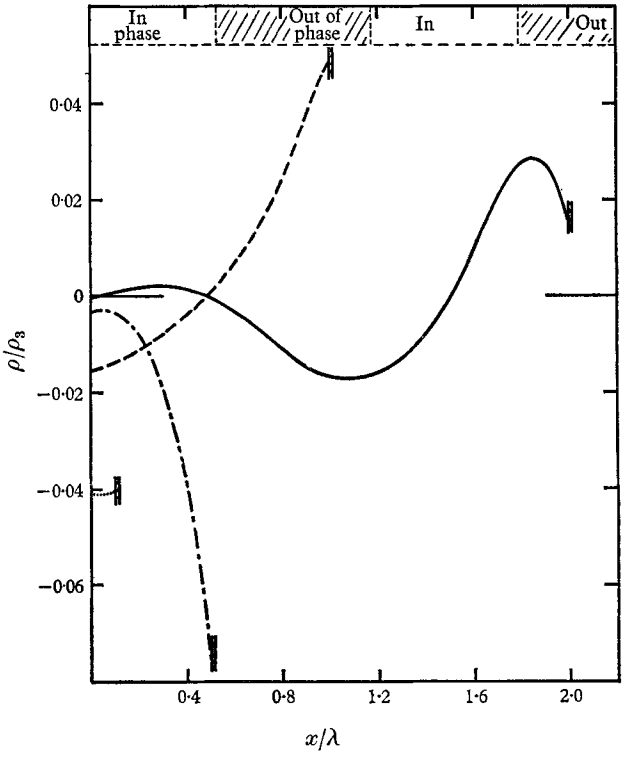

FIGURE 4. Theoretical distribution of perturbation density for several positions of reflected shock-front; incident Mach number is 1·404.

An additional result, derived by Briscoe (1967), gives the perturbation density in the reflected region. The perturbation density is not given by the isentropic formula since the reflected shock-strength varies with y and t; however, the entropy perturbation is only a function of x and y by the last of equations (2.1); thus, the local density perturbation in a fluid element depends upon the entropy perturbation received by it at an earlier time due to the passage of the non-uniform reflected front; we can get

$$\overline{\rho}(\xi, x_s) = \frac{\rho_3}{c_3} \sum_{n=0}^{\infty} B_n \frac{(1+\beta\xi)^{2n+1} + (1-\beta\xi)^{2n+1}}{(1+\beta)^{2n+1} + (1-\beta)^{2n+1}} \left(\frac{1-\beta^2}{1-\beta^2\xi^2}\right)^{n+\frac{1}{2}}$$
$$\times J_{2n+1}\left[\frac{kx_s}{\beta}(1-\beta^2\xi^2)^{\frac{1}{2}}\right] + \left(\frac{E}{B} - c_3^{-2}\right)\rho_3 c_3 \sum_{n=0}^{\infty} B_n J_{2n+1}\left[\xi\frac{kx_s}{\beta}(1-\beta^2)^{\frac{1}{2}}\right], \quad (2.22)$$

where $\xi = x/x_s$. Note that B_n has the dimensions of velocity.

Equation (2.22) is plotted for several instants of time in figure 4. These results will be seen to be in good qualitative agreement with the experimental data.

3. Extension of linearized theory to arbitrary wall shapes. Specific result for a Gaussian wall

The formulation in §2, as given by (2.1), (2.2), (2.3), (2.5) and (2.6) is not restricted to sinusoidal walls. The initial conditions, equations (2.4), must be specified, but need not be sinusoidal. For example, it may be some other periodic function; or it may be non-periodic. The periodic initial shape is appropriately treated by Fourier series techniques; the non-periodic initial shape can be analysed using the Fourier transform. We shall treat the non-periodic problem only since one of our experimental results concerns a Gaussian wall.

The Fourier transform is defined by

$$f^*(k) = \frac{1}{\sqrt{2\pi}} \int_{-\infty}^{+\infty} f(x)\, e^{-ikx}\, dx;$$

its inverse is given by

$$f(x) = \frac{1}{\sqrt{2\pi}} \int_{-\infty}^{+\infty} f^*(k)\, e^{ikx}\, dk.$$

The requirements for the existence of $f^*(k)$ and its inverse are discussed by Morse & Feshbach (1953, p. 456), for example.

If the system of equations (2.1), (2.2), (2.3), (2.5) and (2.6) is Fourier transformed with respect to y, a new system is obtained for the new dependent variables p^*, u^*, v^* and s^* with independent variables x, t and parameter k; this system is identical in form to that resulting from replacing all dependent variables $F(x, y, t)$ by $\bar{F}(x, t)\exp(iky)$. This being the case, we may write down the solution for a chosen k; the Fourier transformed shock shape is, in analogy to (2.21),

$$\psi^*(r_s; k) = \psi^*(0; k)\left[J_0(r_s) + \sum_{n=1}^{\infty} D_n J_{2n}(r_s) \Big/ \sum_{n=0}^{\infty} B_n\right]$$

where, we recall,

$$r_s(t; k) = (kU_r t/\beta)(1-\beta^2)^{\frac{1}{2}}.$$

The inverse yields

$$\psi(y, t) = \frac{1}{\sqrt{2\pi}} \int_{-\infty}^{+\infty} \psi^*(r_s; k)\, e^{iky}\, dk, \tag{3.1}$$

where

$$\psi^*(0; k) = \frac{1}{\sqrt{2\pi}} \int_{-\infty}^{+\infty} \psi(y, 0)\, e^{-iky}\, dy. \tag{3.2}$$

If the wall is given by the Gaussian $x_w(y) = \epsilon \exp(-y^2/2\sigma^2)$, then the initial shock shape is assumed to be

$$\psi(y, 0) = \epsilon(1 + U_r/U_i) \exp(-y^2/2\sigma^2); \tag{3.3}$$

ϵ is the maximum height, and σ is the standard deviation of the Gaussian. Equation (3.2) may be integrated to yield

$$\psi^*(0; k) = \sigma\epsilon(1 + U_r/U_i) \exp(-k^2\sigma^2/2). \tag{3.4}$$

The integration of (3.1) involves integrals of the form

$$\int_0^{\infty} J_\nu(at) \exp(-p^2t^2)\, t^{\mu-1}\, dt$$

after $\exp(iky)$ is expanded as a power series in ky; Watson (1966, p. 394), discusses and evaluates them. The computation is much simpler if we content ourselves with $\psi(0,t)$; we require

$$\int_0^\infty J_{2\nu}(at)\exp(-p^2t^2)\,dt = \frac{\sqrt{\pi}}{2p}\exp(-a^2/8p^2)\,I_\nu\frac{a^2}{8p^2}, \tag{3.5}$$

a result given by Watson (1966), where $I_\nu(\eta) = (i)^{-\nu}J_\nu(i\eta)$. Then (3.1) can be put in the form

$$\frac{\psi(0,t)}{\psi(0,0)} = e^{-w}I_0(w) + \sum_{n=1}^{\infty} D_n e^{-w}I_n(w)\Big/\sum_{n=0}^{\infty} B_n, \tag{3.6}$$

where

$$w \equiv (x_s/2\sigma\beta)^2(1-\beta^2). \tag{3.7}$$

For the Gaussian wall, the standard deviation σ plays the same role as the wavelength λ of the sinusoidal wall. Several computations of (3.7) are shown in figure 5; the decay of the peak amplitude is now monotonic as contrasted with the damped oscillation for the sinusoidal perturbation shown in figure 3. This contrast is supported by the experimental results.

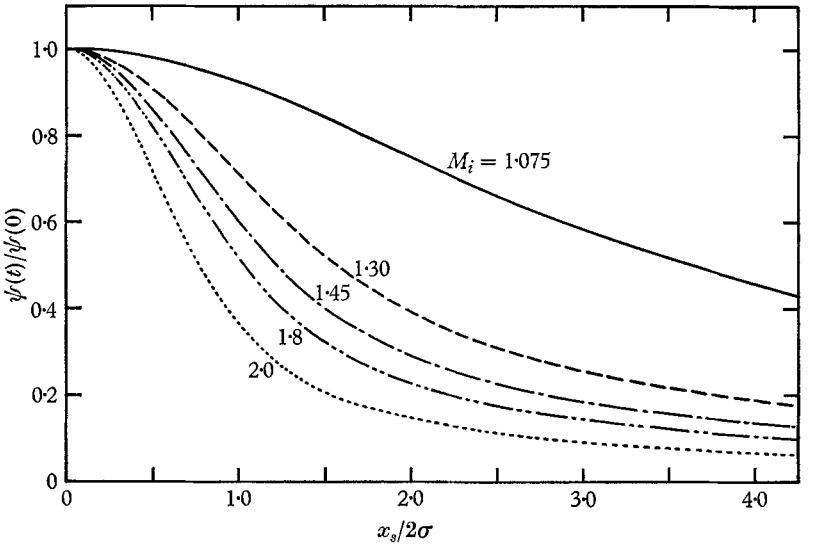

FIGURE 5. Theoretical perturbation damping for shock reflexion from a Gaussian wall.

4. Experimental apparatus

Figure 6 is a schematic diagram of the experimental apparatus. The shock wave is produced by a conventional, rectangular cross-section, diaphragm shock tube; the dimensions are 1 in. by 3 in. with a compression chamber length of 37 in. and an expansion chamber length of 61 in. The test section has 1 in. thick plexiglass windows and is 24 in. long. The diaphragms are cellulose acetate of thickness 0·0015 in. and 0·005 in., depending on the Mach numbers desired; they are ruptured by an air-actuated needle on the expansion-chamber side of the diaphragm.

Compressed air provides the compression-chamber pressure; the expansion chamber operates at ambient conditions. Although this arrangement limits the pressure ratios and the Mach numbers obtainable, and requires one to use air as a working medium, it contributes much simplicity to the experiment.

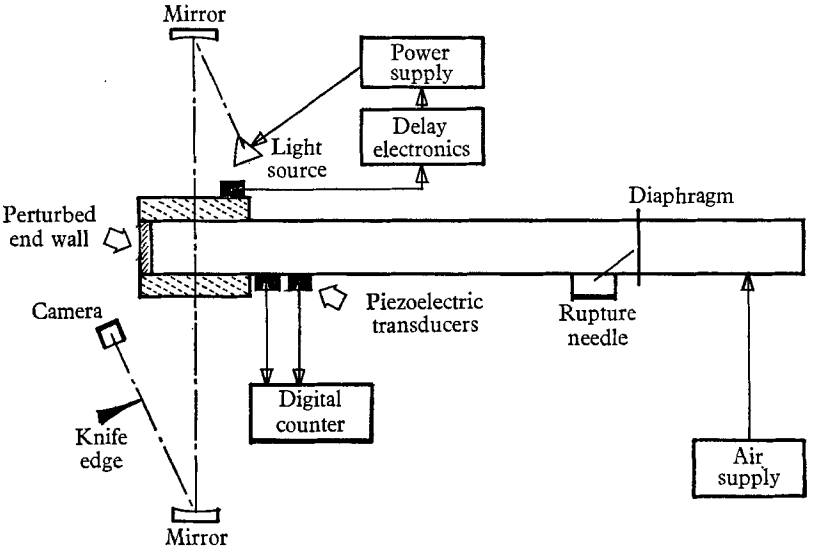

FIGURE 6. Schematic diagram of the experimental apparatus.

Two barium-titanate, piezoelectric transducers next to the test section monitored the incident shock speed; their outputs were amplified and used to start and stop a digital counter. Another transducer near the end of the test section provided the signal to start the delay electronics used to trigger the photographic system. A Rutherford A-11 delay unit gave digital delays from 0·1 μs to 1 s. System jitter was less than 2 μs on an average delay time of about 200 μs.

An EG and G stroboscope with two discharge units was triggered at the desired instant by the delay electronics. The interval between the flashes was determined by a variable oscillator; by continuously hetrodyning the variable oscillator against a crystal oscillator and observing the beat note, the interval between flashes was measurable within a few parts per million. A standard double-mirror schlieren system with a vertical knife-edge made visible the density gradients in the test section; 45 in. focal length mirrors and a 1 mm width of the light-source slit provided high sensitivity. The pictures were recorded on 35 mm Kodak Plus-X film and developed normally in D-76. The magnification of the test section on the film was about 1/3; data were measured from the negatives with an optical comparator having 20 $\times$ enlargement on the viewing screen and a traversing table movable in two dimensions by micrometers calibrated in ten-thousandths of an inch.

One picture was taken per diaphragm rupture; the two-flash stroboscope allowed the measurement of shock perturbations at two shock positions and indicated the speed of the mean location of the wavy reflected shock between the two positions. Repeatability of measured incident-shock speed was within

3%, and measured reflected-shock speed was within 4%. The sinusoidal perturbations were placed on the shock front by wavy blocks mounted in the end of the test section; the blocks were machined according to templates scaled down from large plots of sinusoids. Three wavy walls were used, all of which had 0·580 in. wavelength and 5 waves; the amplitudes were 0·015, 0·029 and 0·058 in. The maximum slopes were approximately 9, 16 and 29 degrees, respectively. The Gaussian wall also was machined from a template; its maximum height was 0·050 in. and its standard deviation was 0·082 in.

Incident Mach numbers were calculated from the measured incident shock speeds and a knowledge of the unshocked conditions in the expansion chamber; this yielded calculated velocities and sound speeds in the flow behind the shock wave, from which the reflected Mach numbers could be calculated once the measured reflected-shock speeds were known.

Tests were run at two conditions; incident Mach numbers were measured as 1·45 and 1·09 and reflected Mach numbers were 1·36 and 1·07, respectively. The corresponding pressures in the compression chamber were 90 and 20 psig.

The measured reflected-shock speeds were found to be about 4% below the calculated speed based on the known incident conditions; this corresponds to decrements in the reflected Mach number of about $2\frac{1}{2}$%. None of the schlieren photographs showed any evidence of reflected shock–boundary-layer interaction as discussed by Mark (1957); this is not surprising in view of the low Mach numbers used for the experiments.

Amplitudes of the perturbations on the shock front were measured along the line $y = 0$; that is, along the line of symmetry half-way between the top and the bottom edges of the test section. Data for the perturbation-damping theory were measured directly from the schlieren negatives†.

A different approach had to be used to obtain the distribution of perturbation density between the reflected shock-front and the wavy wall. One end of a fibre-optic cable was fastened to the centre of the screen on the optical comparator and the other end connected to a photomultiplier-amplifier system; as the movable table on the comparator was traversed so as to scan the negative underneath the fibre optic, the output of the amplifier gave a voltage reading linearly proportional to the intensity of the light passing through the schlieren negative. Because the negative opacity is linearly related to the amount of illumination striking the film (an approximation that assumes that a mean illumination level exposes the film to a mean opacity), and because the amount of illumination striking the film is linearly related to the density gradients in the test section (assuming that integration and diffraction effects are negligible, an approximation that is not too good), this scan of the negative opacity by the optical comparator-photomultiplier system produces a plot that is directly related to the distribution of perturbation density in the test section. The plot needs two calibration factors to specify it completely; the perturbation density that corresponds to the mean illumination level passing through the negative, and a number that gives the change in perturbation density for a given change in negative

† Single-flash schlieren pictures were used as data sources for the density-distribution measurements.

opacity. Because these two calibration factors were not readily available, but mainly because the density distribution was not of major interest to this study, we were content with plotting the experimental distribution of perturbation density against the theoretical distribution and forcing the vertical heights of the end-points of the two curves to match. The final data plots, discussed in the next section, are therefore only qualitative presentations to show that the *shape* of the distribution curves in theory and experiment are reasonably well matched.

Error bars on the data curves are calculated from two factors; measured scatter in the speed measurements, and estimated errors in the optical comparator measurements of the perturbation amplitudes on the schlieren negatives. The bars are of such a height that they represent a confidence interval of 50%; that is, if the data are scattered normally about the mean value, then half of the data would fall inside the confidence interval.

5. Experimental results and discussion

Plate 1 shows a typical sequence of schlieren photographs illustrating the oscillating and damping process for the perturbations on the reflected shock front. The two flashes of the stroboscope occurred 10 μs apart, the wall had an amplitude of 0·015 in., the incident Mach number of the shock was 1·45. The second and third pictures in the sequence indicate the oscillating behaviour of the perturbations. Note that even for this slightly sloped wall the reflected shock is not sinusoidal after it has travelled a short distance from the wall; the theory, in essence, predicts the damping of the first term in a series expansion (of the initial reflected shock-shape). It appears that the non-sinusoidal reflected shock-shape is caused by the higher order terms. In any case, because the higher-frequency terms damp sooner, the dominant term in the series expression for the reflected shock-shape at any time is still the lowest order term; that is, we expect the total amplitude of the reflected shock at any time to be closely approximated by the amplitude of the lowest harmonic in the shape, the same harmonic that is described by the theory of §2.

Plate 2 shows shock reflexion from a steeply sloped wavy wall (amplitude 0·058 in); the incident Mach number was 1·45. Note two significant differences between the steeply sloped-wall reflexion and the slightly sloped-wall reflexion: the initial shock-shape in the former is not sinusoidal at all, and the pattern of disturbances behind the reflected shock is much more distinct (and, thus, stronger) for the steep-wall reflexion. Plate 3 indicates the sequence of reflexion from a Gaussian wall; again, the incident Mach number is 1·45. The most striking feature of these photographs is the absence of oscillation of the shock shape. These last pictures show especially well the corner-waves issuing from the non-perfect intersection of the shock-tube walls and nearly flat end-wall; since the perturbation-amplitude measurements are taken along the centre line of the shock tube, the corner-waves have no effect on the data until they have touched the centre of the reflected shock. This does not occur until the shock has passed out of the field of view of the schlieren system.

The curves are a plot of non-dimensional perturbation amplitude (amplitude at a given time divided by initial amplitude) versus non-dimensional distance from the wall (actual distance, $x_s = U_r t$, divided by the wall wavelength or the Gaussian standard deviation).

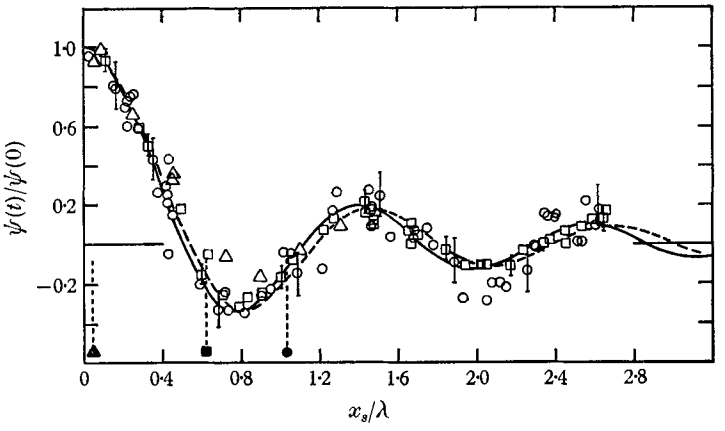

FIGURE 7. Comparison of experimental and theoretical results for reflexion from a sinusoidal wall; measured incident Mach number (solid line) 1·45, measured reflected Mach number (broken line) 1·36. Circle data points are for amp/wavelength of the wall equal to 0·026; squares for 0·050 wall; triangles for 0·100. Vertical dotted lines indicate the point beyond which the reflected front no longer appears to be sinusoidal.

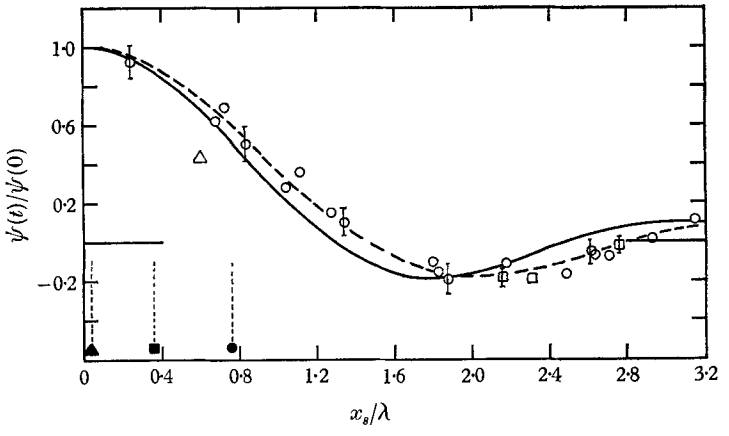

FIGURE 8. Comparison of experimental and theoretical results for reflexion from a sinusoidal wall; same legend as figure 7. $M_i = 1{\cdot}09$, $M_r = 1{\cdot}07$.

Figure 7 gives the experimental results for measurements of the amplitude of perturbations on a shock wave that has been reflected normally from a sinusoidal wall; the incident Mach number was 1·45 in air. The three different plotting symbols refer to data from wavy walls of three different amplitudes; circles correspond to 0·0015, squares to 0·029, and triangles to 0·058 in. amplitude. The wavelength was 0·580 in. for all three walls. The vertical dotted lines indicate the approximate point beyond which the reflected shock no longer appeared to

be near-sinusoidal. The plotted curves are the theoretical perturbation damping curves based on the measured incident Mach number (1·45, solid line) and the measured reflected Mach number (1·36, dotted). Figure 8 is the same type of presentation but for 1·09 and 1·07 incident and reflected Mach numbers, respectively.

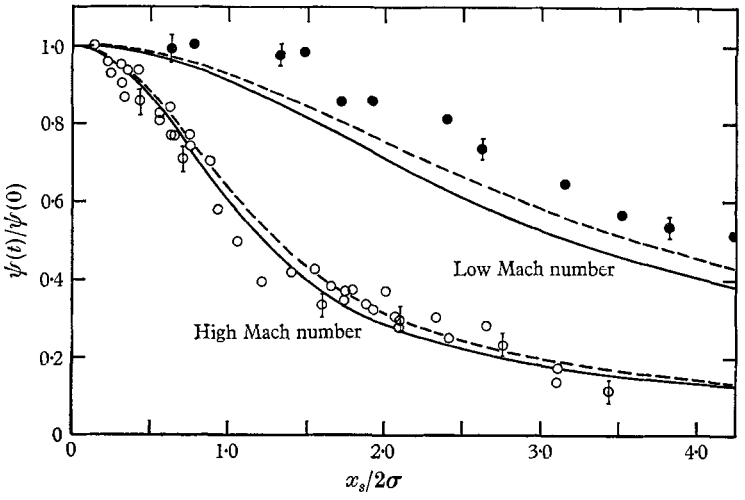

FIGURE 9. Comparison of experimental and theoretical results for reflexion from a Gaussian wall; lower curves for $M_i = 1{\cdot}45$ and $M_r = 1{\cdot}36$; upper curves for $M_i = 1{\cdot}09$ and $M_r = 1{\cdot}07$.

Figure 9 gives the experimental results for both sets of Mach numbers for the shock reflexion from a Gaussian wall. Again, the solid and dotted curves refer to the theoretically predicted damping based on the measured incident and reflected shock speeds, respectively.

Figure 10 shows the qualitative agreement between theory and experiment for the distribution of perturbation density between the wavy wall and the reflected shock front. As discussed in §4, the starting point and total spread of the data were forced to fit the theory; only the general shape of the curves are to be compared.

For the wavy wall reflexions, the predicted curves and the data are in excellent agreement, especially for the locations of the zero-crossing; note that the dotted theoretical curve (based on the measured reflected Mach number) fits the data better. The data for the least-sloped wall (circle data-points) show amplitude variations that are somewhat larger than predicted; this indicates that the 'tension' of the shock shape (if the shock is thought of as an oscillating, semi-permeable membrane) is less in the real case than in the mathematical model of a step-shock. This is possibly due to the finite thickness of the real shock, or to the presence of shear stresses that hinder the transverse propagation of perturbations (the mechanism of free-space shock stability).†

It is seen from the comparison of the data for the three different wavy walls

† See a forthcoming paper by the authors on 'Free-Space Damping of Perturbations on a Plane Shock Wave'.

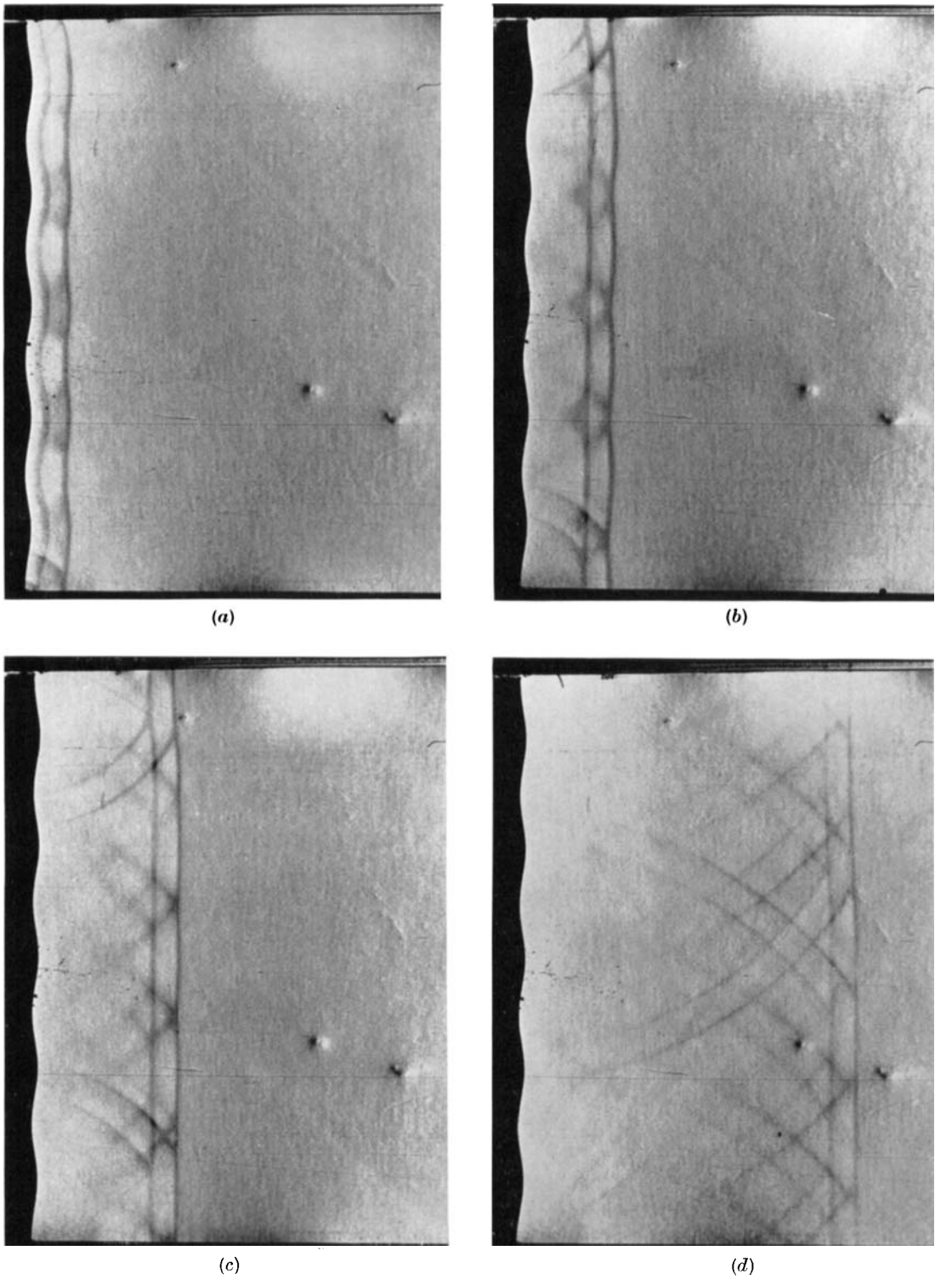

PLATE 1. Sequence of two-flash stroboscopic schlieren photographs showing damping and oscillating behaviour of reflected front; reflected front moves from left to right; time interval between flashes, 10 μs. Sinusoidal wall has 0·015 in. amplitude and 0·580 in. wavelength; incident Mach number is 1·45.

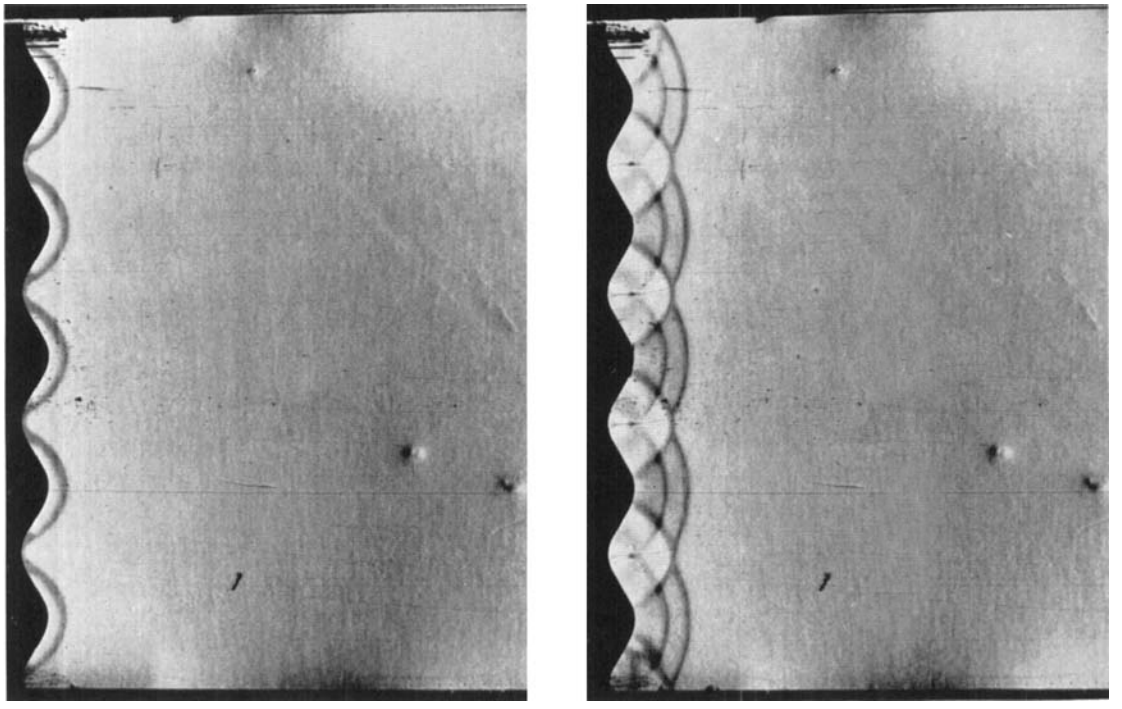

(*a*) (*b*)

PLATE 2. Sequence of two-flash stroboscopic schlieren photographs showing reflexion from a steeply sloped sinusoidal wall; 0·048 in. amplitude and 0·590 in. wavelength; incident Mach number is 1·45; reflected front moves from left to right; time interval between flashes, 10 μs.

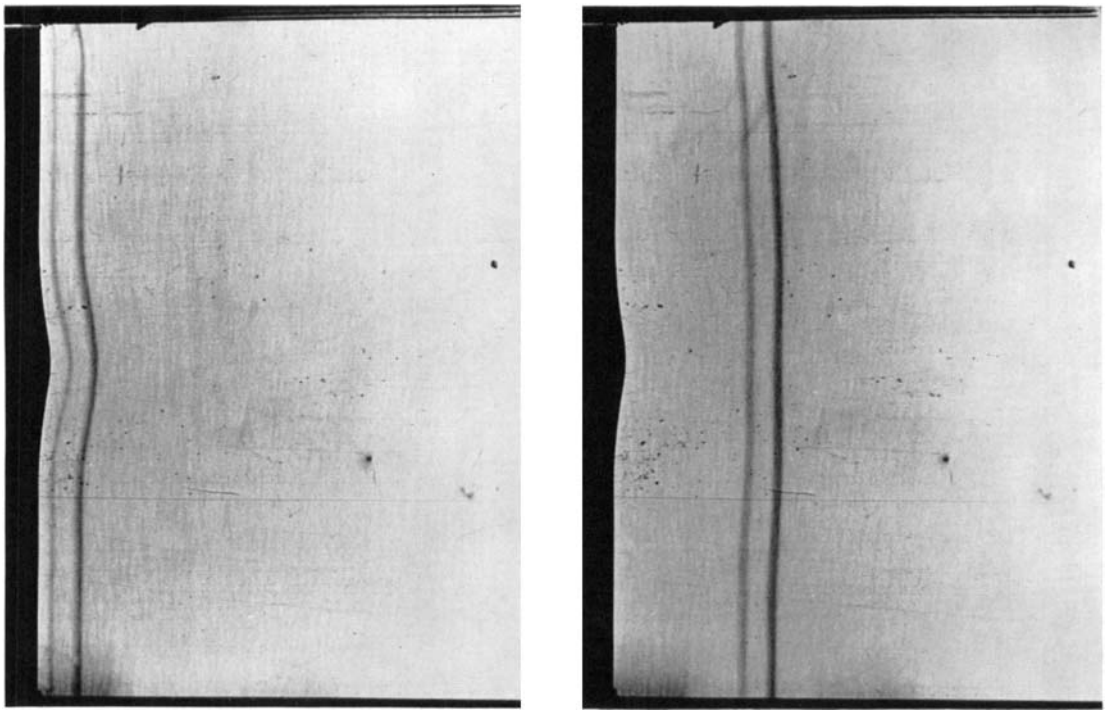

(*a*) (*b*)

PLATE 3. Sequence of two-flash stroboscopic schlieren photographs showing reflexion from Gaussian wall; 0·050 in. peak amplitude; 0·182 in. standard deviation; incident Mach number is 1·45; reflected front moves from left to right; time interval between flashes, 10 μs.

that non-linearities in wall slope (steep walls) seem to affect the damping rate in two ways: the extremals of the oscillations become smaller and smaller, and the frequency of oscillations becomes slightly faster.

We are unable to explain the relatively poor agreement between theory and experiment for the low Mach number Gaussian wall data. The wavy wall data for the same Mach number show excellent agreement. It is interesting that Lapworth's low Mach number data was worse than the higher Mach number results; his experiment involved a non-sinusoidal shock also.

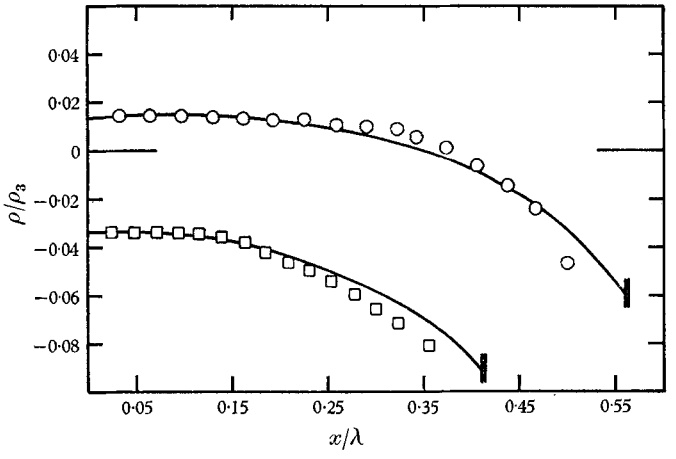

FIGURE 10. Comparison of experimental and theoretical results for distribution of perturbation density between sinusoidal wall and reflected shock-front; amp/wavelength of wall is 0·026; incident Mach number is 1·45.

6. Conclusions

We have shown excellent agreement between a linearized theory for the damping of perturbations on a shock wave reflected from a nearly flat surface and shock-tube experiments for shock reflexion from sinusoidal and Gaussian walls. Since the perturbation damping behaviour is dependent on the medium through which the shock is moving, it appears that the reflexion theory could be used as a diagnostic technique to obtain information about the state of the fluid medium; a possible example would be a simple chemically reacting system through which a perturbed shock wave is propagated and its damping behaviour observed.

The experiments only tested the theory for relatively low Mach numbers, primarily because real shock-tube effects that were not considered in the theory would have arisen at any higher Mach numbers than the ones used (specifically the boundary-layer reflected shock interaction that is a necessary part of shock-tube experiments in the medium-Mach number régime). It is likely that high Mach number experiments would, of necessity, have to be modelled by a theory that accounts for chemical reactions and changing gas properties.

The discussions with Prof. Severin Raynor and the machine shop work of Messrs Robert Klaub and William Rahm are gratefully acknowledged.

REFERENCES

BLACKBURN, D. 1953 Unsteady perturbations of strong shock waves. Ph.D. Thesis, Manchester University.

BRISCOE, M. G. 1967 Normal shock reflection from nearly flat walls. Ph.D. Thesis, Northwestern University.

COURANT, R. & FRIEDRICHS, K. O. 1948 *Supersonic Flow and Shock Waves.* New York: Interscience.

FREEMAN, N. C. 1955 A theory of the stability of plane shock waves. *Proc. Roy. Soc.* A **228**, 341–62.

FREEMAN, N. C. 1957 On the stability of plane shock waves. *J. Fluid Mech.* **2**, 397–411.

LAPWORTH, K. C. 1957 An experimental investigation of the stability of plane shock waves. *J. Fluid Mech.* **2**, 341–62.

LIGHTHILL, M. J. 1949 The diffraction of blast. I. *Proc. Roy. Soc.* A **198**, 454–70.

LIGHTHILL, M. J. 1950 The diffraction of blast. II. *Proc. Roy. Soc.* A **200**, 554–65.

MARK, H. 1957 The interaction of a reflected shock wave with the boundary layer in a shock tube. Ph.D. Thesis, Cornell University. NACA-TM-1418 (1958), AFOSR-TN-57-345, AD-132-418.

MORSE, P. M. & FESHBACH, H. 1953 *Methods of Theoretical Physics.* New York: McGraw-Hill.

NIKOLAEV, IU. M. 1965 Solution for a plane shock wave moving through a lightly curved interface of two media. *J. Appl. Math. Mech.* **29**, 785–94.

SAKHARNOV, A. D., ZAIDEL, R. M., MINEEV, V. N. & OLEINIK, A. G. 1965 Experimental investigation of shock waves and the mechanical properties of substances at high pressures and temperatures. *Soviet Physics-Doklady*, **9**, 1091–4.

WATSON, G. N. 1966 *A Treatise on the Theory of Bessel Functions.* 2nd edition. Cambridge University Press.

ZAIDEL, R. M. 1960 Shock wave from a slightly curved piston. *J. Appl. Math. Mech.* **24**, 316–27.